Journal of Diabetes Science and Technology
2018, Vol. 12(6) 1159–1168

DOI: 10.1177/1932296818763457
journals.sagepub.com/home/dst
SAGE

Device and Method for Noninvasive Glucose Assessment

Yosef (Joseph) Segman, PhD[1]

Abstract

Background: Intensive monitoring of blood glucose levels is crucial in diabetes management. This article presents a new device, the TensorTip Combo Glucometer (CoG), developed by Cnoga Medical Ltd, which enables to predict capillary tissue glucose concentration noninvasively.

Methods: Noninvasive glucose readings usually provide irregular or disordered mathematical manifold over the measurement space. To establish a transfer function, which correctly correlates the noninvasive raw data and the actual invasive glucose level, we suggest a mathematical concept that employs a personal calibration procedure to associate glucose pattern and multiple optical signals derived from tissue response to light emission in the range of visible to IR. The traversed light is detected by a color image sensor to predict the tissue glucose concentration at the fingertip. This article presents the mathematical concept underlying the technology and the requirements for device operation.

Results: The device was clinically evaluated and compared to standard invasive blood glucose monitoring devices in few medical centers and by home users. Based on consensus error grid analysis, more than 98% of the measurements of each study were in zones A (more than 81%) and B (more than 11%). Postmarketing evaluations showed high correlations comparing the CoG to other invasive reference devices.

Conclusions: The CoG device employs a unique mathematical approach to predict glucose concentrations based on multiple optical signals. The first clinical results indicate that the device may show appropriate agreement with reference methods to be used for pain-free glucose assessment in daily routine.

Keywords

Cnoga TensorTip Combo Glucometer, CoG, noninvasive tissue glucose monitoring, visual and near infrared light source, fingertip, diabetes

Diabetes is a global health burden, declared by World Health Organization as a global epidemic due to its rapidly growing prevalence.[1] It is a chronic disease in which glucose levels are increased in the body due to either insufficient insulin production by the pancreas or un-effective usage of insulin by the body. The sequelae of insufficiently controlled diabetes with frequent hyperglycemia includes long-term damage, dysfunction and failure of various organs including the retina, kidney and vasculature.[2] Intensive management of blood glucose levels is crucial for a good long-term outcome in diabetes health care. The Diabetes Control and Complications Trial and the UK Prospective Diabetes Study follow-up showed that early, tight glucose control in people with type 1 and type 2 diabetes reduced the risk of development or progression of long-term diabetes complications.[3,4]

Today, the finger stick testing is the mainstay of blood glucose detection. Sufficient blood glucose monitoring requires frequent blood measurements accompanied by discomfort and pain.[5,6]

The need for convenient blood glucose self-monitoring technique has led to the development of alternative technologies including needle sensors for continuous glucose monitoring and noninvasive monitoring devices. Continuous blood glucose devices require invasive sensors to be inserted under the skin and being replaced at least twice a month, which is inconvenient and expensive.[7-10]

So far, several noninvasive methods including near infrared spectroscopy, Raman spectroscopy, ultrasound and so forth were proposed, however no satisfactory solution was introduced to the market.[11-14] Optical methods have failed to recognize blood glucose level mainly because glucose has weak connection to light, for example, visible to IR light. Furthermore,

[1]Cnoga Medical Ltd, Caesarea North Industrial Park, Caesarea, Israel

Corresponding Author:
Yosef (Joseph) Segman, PhD, R&D, Cnoga Medical Ltd, Caesarea North Industrial Park, 5th Tarshish St, POB 3188, Caesarea, 3088900, Israel.
Email: Yosef@cnoga.com

glucose represents less than 0.1% of human tissue by weight. Therefore, variances due to thermal, mechanical, hemodynamics, optical or other instabilities may interfere with the noninvasive glucose reading.[15] Kromoscopic analysis was investigated as a possibility for a spectroscopic analysis to measure glucose noninvasively. Even though the device did respond to glucose, still instrumental improvements were needed to increase the sensitivity and concentration resolution.[16,17] A different approach, done lately by Yamakoshi et al, is using a technique named photoplethysmography, which can provide significant physiological information that can be derived from the signal produced, the photoplethysmogram (PPG). They have measured successfully the simultaneous PPGs, among them few optical absorption bands of glucose. Although this system is very useful for research, it is still not suitable for routine clinical use, such as in the case of diabetes self-monitoring.[18,19] A new prototype[20] that uses near infrared transmission spectroscopy has also been investigated. In this research they found a correlation between the sensor output voltage and the glucose concentration levels. This device is not available in the market, and more research and development need to be accomplished. As far as we are aware, none of them have reached the level of market-approved device.

This article presents a new method, based on a neural brain network (NBN), in which the model is based on response of synchronized group of neurons. The method presented in this article does not focus on the glucose molecule, rather on real-time color photography related to the glucose levels in the capillary tissue. These real-time images, which are connected to a momentary glucose level are transform into vector whose components acquired from the color image sensor and are being used as neurons capable to identify pattern of tissue glucose concentration noninvasively. The measurements are taken at different times during the day reflecting a semicontinuous glucose monitoring mechanism. The technology is based on several assumptions (detailed in the mathematical model in the Methods section), enabling overcoming the difficulties encountered by previous optical methods.

Methods

The TensorTip Combo Glucometer (CoG)

The new device for invasive and noninvasive glucose assessment is small, light-weight and portable device, as can be seen in Figure 1a. The device is intended for use in the home environment or as an additional support in clinics. The device consists of medical technology and control subsystems. The medical technology subsystem contains a color image sensor, LEDs, and a digital signal processor (DSP), which is responsible for the image acquisition, the image processing, the lighting control system, and the extraction of the clinical parameter results. The control subsystem contains four touch buttons, a display, an audiospeaker, and a microcontroller,

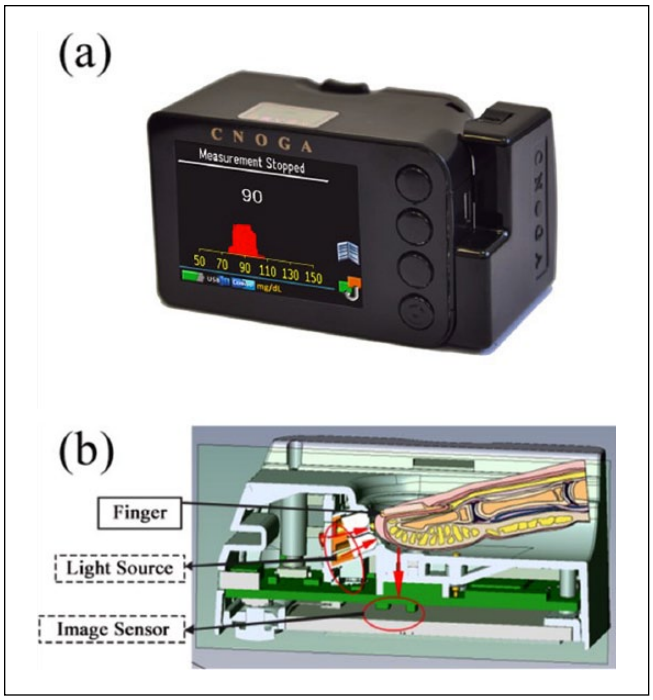

Figure 1. (a) The CoG device. (b) A cross-sectional view of the CoG.

which is in charge of the user interface, the process management, the internal storage, and the device's power management. As shown in Figure 1b, the device employs a finger compartment, four monochromatic light sources in the visual to IR spectrum (~600 nm to ~1000 nm), a color image sensor, and a conventional invasive glucometer as add-on module. The invasive add-on module is technically identical to the approved Okmeter match device K090609 (OK Biotech Co, Ltd, Hsinchu City, Taiwan). The add-on module is used for calibration of the noninvasive component. As described in the patents issued by the company,[21-26] the technology of the noninvasive device component is based on a real-time color image sensor, which provides the ability to analyze capillary blood tint over spatial-temporal-color domain. The CoG color image sensor provides richer information compared to other known devices, such as a standard pulse oximetry (see the appendix). A pulse oximeter usually uses two discreet diode sensors and two monochromatic light sources.[27-29] The device uses four monochromatic light source and color image sensors absorbing continuous wavelength light usually in the range from visible blue to IR. There is no special index to the traverse light as it diffuses over the entire range of the image sensor; therefore, all three color hyperplanes (red, green, and blue) will sense the traverse light, each one with a different sensing efficacy. The color image raw data are stored in a memory buffer to be used for the computation of a dedicated algorithm executed in the device DSP component. A short description of the device technology and its components is described elsewhere.[30]

The Underlying Mathematical Model

The most difficult part in developing a noninvasive biomarker reading is the isolation of the biomarker by the algorithm. This is achieved by associating a vector V to a single glucose level. The vector components are based on the information gathered by the color image sensor. The following basic assumptions are used for the device algorithm:

a. **Isolation:**

Two nonidentical vectors representing temporary light absorption traverses the tissue under consideration may represent identical or almost identical glucose levels. However, two identical or almost identical vectors will definitely represent a single glucose level.

b. **Calibration:**

Personal calibration is achieved by designing optimal personal preschedule glucose readings. Momentary blood tint may vary between people and within each person during the day. At the current status we recommend on at least 25 prescheduled calibration of reliable references (each reference test is using two strip readings) generated from measurements taken at different hours of the day, for several days. The personal calibration range is designed in a way that it covers the personal glucose range. The device may predict glucose level outside the personal calibration range.

During the calibration period, two standard-conventional strips for "double-check" per each noninvasive sample vector V are used as reference. To avoid additional pain, once cleaning the area the second whole blood sample can be withdrawn from the same pricking site. During personal calibration the device will provide noninvasive results once it collects a sufficient data, usually it occurs after three invasive references. A successful calibration process would achieve the most accurate personal glucose pattern. If the two strip readings are not sufficiently close to each other, the noninvasive sample vector is internally declared by the system as "bad reference." The advantage of personal calibration versus universal calibration is that the personal pattern takes individual interfering factors into consideration.

Personal Calibration Process Description. The calibration is a process of prescheduled noninvasive data collection represented by a set of vectors versus true invasive glucose readings. Each noninvasive reading produces a sample vector V_k, associated with two invasive blood glucose measurements using standard-conventional strips sufficiently close to each other (g_{k1} and g_{k2}). This association is considered as the "isolation mechanism" of the capillary tissue glucose, that is,

$$V_k \leftrightarrow \left(g_{k1},\ g_{k2}\right) \tag{1}$$

A fundamental requirement of (1) is the independency of the set of vectors $\{V_k\}$. Independency means that there are no two vectors sufficiently close to each other, that is, $V_k = V_n$ for $k \neq n$, resulting with two different glucose levels. In mathematical terms:

$$\text{If } V_k = V_n \text{ then } g_k = g_n \text{ for any } k \neq n \tag{2}$$

where g_k and g_n are the actual glucose level references acquired by the add-on invasive device component.

Constructing a Vector V_k

1. Let $r_n(x,y,t)$, $g_n(x,y,t)$ and $b_n(x,y,t)$ be the three spatial-temporal-color video stream representing the absorption levels of the capillary tissue under consideration illuminated by a set of monochromatic light (L_{in}) having emission levels (e_{in}). i represents a wavelength index ($1 \leq i \leq 4$) and n represents a set of light combination ($1 \leq n \leq N$).

Example:

i = 1,2,3,4; n = 1

- L_{11} = 625 nm LED emitted at e_{11} milliamp
- L_{21} = 740 nm LED emitted at e_{21} milliamp
- L_{31} = 850 nm LED emitted at e_{31} milliamp
- L_{41} = 940 nm LED emitted at e_{41} milliamp

i = 1,2,3,4; n = 2

- L_{12} = 625 nm LED emitted at e_{12} milliamp
- L_{22} = 740 nm LED emitted at e_{22} milliamp
- L_{32} = 850 nm LED emitted at e_{32} milliamp
- L_{42} = 940 nm LED emitted at e_{42} milliamp

Each set of light n corresponds to a set of real-time images $r_n(x,y,t)$, $g_n(x,y,t)$ and $b_n(x,y,t)$ wherein for n = 1 $r_1(x,y,t)$, $g_1(x,y,t)$ and $b_1(x,y,t)$ and for n = 2 $r_2(x,y,t)$, $g_2(x,y,t)$ and $b_2(x,y,t)$.

2. Let U_{kn} be a feature-vector associated with invasive whole blood glucose level g_k and a set of lights n = 1 … N. k denotes the index of the k^{th} feature vector in the device log file.
3. Let V_k be a feature-vector composed by $\{U_{kn}\}$, that is, $V_k = (U_{k1}, U_{k2}, U_{k3}, \ldots, U_{kn})$. Taking under consideration the upper example, the vector V_1, that is, k = 1, is composed by two subvectors U_{11} and U_{12}, that is, $V_1 = (U_{11}, U_{12})$, where the subvector U_{11} represents the absorption response to L_{i1} set of light emission and U_{12} to L_{i2} set of light emission.

Adaptive Machine Learning (the NBN). Noninvasive signals are chaotically related to glucose over the Euclidean R^n space. Therefore, an association approach which imitates the NBN is suggested. The following provides some of the major general rules of the NBN system:

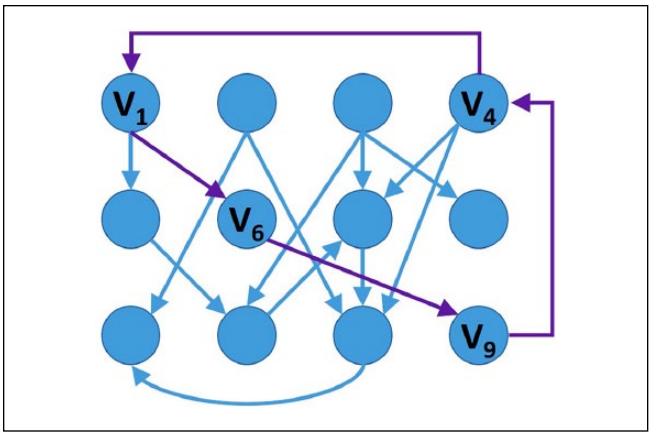

Figure 2. Example of a closed-loop vector association.

1. Valid sample vector:

A vector V_k associated with two invasive references is a valid sample vector if the two references are sufficiently close to each other and the vector itself passes all the internal requirements to internally declare its validity.

2. The NBN components:

The NBN is created by pairing vectors into a branch and forming multiple branches into loops, wherein two vectors are paired if they have a predefined similarity in the blood glucose levels that each is associated with.

Branch: Association of pair of vectors. This association may have a weight representing the connection strength.

Closed loop: Branches that end within one of the previous vectors in the loop, for example, $V_1 \rightarrow V_6 \rightarrow V_9 \rightarrow V_4 \rightarrow V_1$, as presented in Figure 2.

Open loop: A set of connected vectors (branches) that does not end in a closed loop.

Tree: A set of branches having a single origin.

Group: A set of connected vectors with an open or closed loop fulfilling certain condition.

Unpaired: Unassociated vectors.

Calibration tests: A learning set includes N prescheduled measurements, whereas N is at least 25, depends on the severity of patient's illness. The calibration process is based on two tests:

1. Calibration incorporating about 70% of the entire valid sample vectors in the learning log file is used to generate neural network. The 30% of the remaining sample vectors are being used for internal blind test and are considered as a set of new vectors $\{V^{new}\}$. This subset is tested and correlated to the optimal loop of vectors in the basic learning set.
   If the blind test on the remaining 30% is passing the required accuracy, then a secondary test is being performed on the entire learning set (70%+30%) as described below.
2. A subset $A_k = (V_1, \ldots, V_{k-1}, V_{k+1}, \ldots, V_n)$ of valid sample vectors excluding the vector V_k is temporarily used to generate a neural network. The excluded vector V_k is now being used for internal blind test and is considered as a new vector V^{new}. The vector is tested and correlated to the optimal loop of vectors in subset A_k. This process is repeated among all other valid sample vectors.

Calibration concluded: Once the two tests (1+2) are passed successfully, the device informs the user that the calibration is concluded and noninvasive readings may be performed.

Recalibration: The device informs the user when to add additional invasive calibration reference which may occur in cases where the glucose prediction is outside the calibration range or automatically according to an internal plan designed by the device based on the calibration structure representing the severity of the illness. Nonetheless, whenever the user adds a new invasive reading it will be added to the learning set for recalibration, unless canceled by the user.

General Notes

1. Noise is a factor we considered as information as long as it produced by the finger.
2. Higher dynamic range would always assist to a better isolation of any bioparameter including glucose.
3. Noninvasive reading, that is, in vivo reading, requires system solution since there is no direct contact with the biomarker under consideration. This means identifying other factors that may assist to isolate and predict noninvasively the bioparameter under consideration.
4. The algorithm used in the initial study presented in this article did not consider the time in which the references of the invasive readings were inserted into the noninvasive device for calibration. This means that noninvasive glucose predication was not dependent on the time that whole blood reference readings were performed.
5. The purpose of the initial studies presented in this article was to have the ability to construct working neural network (ie, Glucose Manifold), which will be used to predict glucose noninvasively, in other words, isolating the glucose noninvasively.
6. The NBN system is an evolving system that can be fed by information gathered from several participants resulting in a clustered or universal calibration or from a single participant resulting in a personal calibration.

Preliminary Clinical Studies

Preliminary Clinical Methods. The preliminary clinical evaluation of the noninvasive device was conducted in three stages

followed by a postmarketing assessment. The purpose of the studies was to evaluate the effectiveness of the noninvasive device component in predicting capillary tissue glucose. Based on the initial studies presented in this article the system solution was improved and additional studies have been performed during the recent years. A clinical study was performed recently at the Pfützner Science & Health Institute, the study summary can be found in this journal.[31]

All studies were performed in accordance with applicable legal and ethical standards. The respective ethical review boards approved the study protocols, and participants signed informed consent prior to any study procedure.

Study 1—Lin & Carmel Daycare Medical Centers in Haifa, Israel. This was the first study of the entire project. It was conducted on ambulatory patients having chronic liver disease, diabetes, and COPD. The study incorporated two steps: The first step, lasting few weeks, collected raw data from the participants to develop a universal (general) calibration manifold, that is, to construct the NBN system. The second step represented the comparison stage in which the calibration manifold was used to predict the noninvasive glucose levels and compared it with invasive readings.

Study 2—Memorial Morristown Medical Center (MMMC, Morristown, NJ). The study was conducted on patients after heart surgery, while staying in the recovery room mostly for 24 hours. All the participants were hospital-bound and bedridden patients. The invasive glucose readings were collected as part of the routine daily monitoring. This stage was completely blinded, that is, with no precalibration, using the same general calibration manifold as in Lin & Carmel Medical Centers.

Study 3—Home Study. Diabetes patients were guided to use the device at home, performing the entire process of personal calibration and postcalibration comparison. In this study each participant received two devices: noninvasive and invasive glucometers. During calibration, the participant manually inserted the invasive values to calibrate the noninvasive device. After calibration the participant compared the noninvasive outcome with the invasive readings in his daily routine. These data were registered in a special form by the user.

Postmarketing evaluation. Limit customers purchased the device and measured themselves at home environment. After the device was calibrated, the users continued measuring themselves routinely, and voluntarily shared their data with Cnoga Medical Ltd for internal investigation and future improvement.

Statistical Analysis Methods. The overall mean absolute relative difference (MARD) was calculated from all data sets obtained in the studies as follows:

$$\frac{1}{N}\sum_{i=1}^{N}\left(\frac{\left|TensorTip\,CoG_i - Ref_i\right|}{Ref_i}\right) \tag{3}$$

(N = number of measurements preformed after the device was calibrated).

In addition, measurements satisfying the following condition: Device readings ≥ Ref were marked as positive mean relative difference (MRD), which was calculated as follows:

$$\frac{1}{N_p}\sum_{i=1}^{N_p}\left(\frac{TensorTip\,CoG_i - Ref_i}{Ref_i}\right) \tag{4}$$

N_p represents the total measurements with positive MRD.

Measurements satisfying the complementary condition, that is, device readings < Ref, were marked as negative MRD, which was calculated as follows:

$$\frac{1}{N_n}\sum_{i=1}^{N_n}\left(\frac{TensorTip\,CoG_i - Ref_i}{Ref_i}\right) \tag{5}$$

N_n represents the total measurements with negative MRD.

In addition to the performance parameters mentioned above, a consensus error grid (CEG) analysis was performed as published previously by Parkes et al and Pfützner et al.[32,33]

Clinical Results

Study 1

Data were collected from 76 patients (36% female, 64% male, age: 58 ± 14 years), resulting in a total amount of 112 paired measurements performed after calibration. The MARD value in comparison with the best reference out of the three reference devices, Accu-Chek Performa (Roche, Indianapolis, IN), Ascensia Contour (Bayer Healthcare, Tarrytown, NY), and FreeStyle (Abbott Laboratories, Alameda, CA), was 17.9% (positive MRD: 19.4% [N_p = 56]; negative: –16.4% [N_n = 56], $\left(N_p / N\right) = \left(N_n / N\right) = 0.5$, giving a symmetrical diffusion around the regression line). Measured glucose levels were 73-380 mg/dL (with an average of 156 ± 64) and 69-402 mg/dL (159 ± 70) for the noninvasive and invasive devices, correspondingly. Of the measurements in this study, 100% were found to be in zones A and B of the CEG (see Table 1 and Figure 3a).

Study 2

Study 2 included 77 patients (female and male with an almost equal distribution, average age above 60 years), giving 77 measurements. The overall MARD, compared to the reference device, i-STAT (Abbott Laboratories, Alameda, CA), was 14.9% (positive MRD: 14.8% [N_p = 39]; negative: –15.0% [N_n = 38]; positive diffusion: 0.51; negative: 0.49, giving a quite symmetrical diffusion around the regression line). Measured glucose levels were 107-214 mg/dL (144 ± 23) and 97-226 mg/dL (147 ± 29) for the noninvasive and invasive devices, correspondingly. Of the measurements in

Table 1. Results of the Consensus Error Grid Analysis of the Three Clinical Preliminary Studies.

	Measurements, n (%)					
	A+B	A	B	C	D	E
Lin & Carmel Medical Centers	112 (100)	91 (81.25)	21 (18.75)	0 (0)	0 (0)	0 (0)
MMMC	77 (100)	68 (88.31)	9 (11.69)	0 (0)	0 (0)	0 (0)
Home study	721 (98.77)	629 (86.16)	92 (12.60)	7 (0.96)	1 (0.14)	1 (0.14)

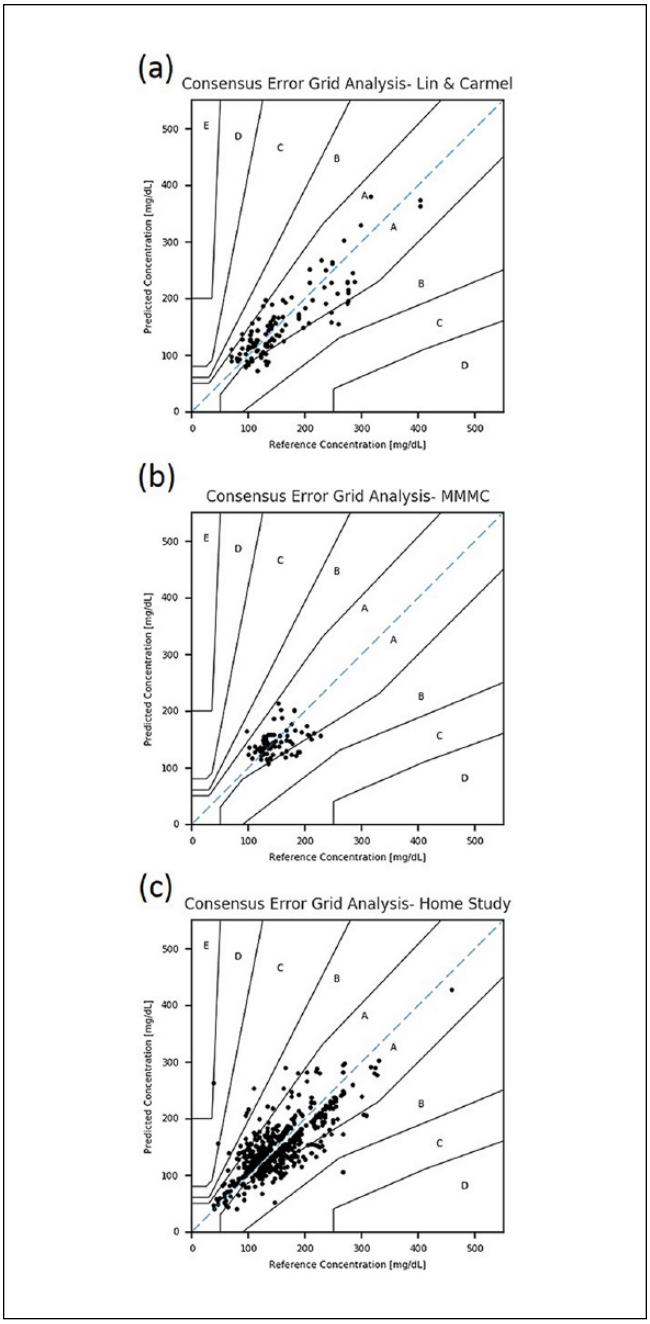

Figure 3. Consensus error grid analysis results of (a) the first clinical study (Lin & Carmel Medical Centers), (b) the second study (MMMC), and (c) the home use study.

this study, 100% were in zones A and B in the CEG, as presented in Figure 3b and Table 1.

Study 3

The home study included 19 participants (21% female, 79% male, age: 55 ± 13 years), and resulted in 730 postcalibration measurements. The overall MARD (compared to home used personal glucometer monitoring devices) was 17.1% (positive MRD: 20.1% [$N_p = 372$]; negative: –13.9% [$N_n = 358$]; positive diffusion: 0.51; negative: 0.49, giving a quite symmetrical diffusion around the regression line). Measured glucose levels were 40-428 mg/dL (145 ± 44) and 37-458 mg/dL (146 ± 49) for the noninvasive and invasive devices, correspondingly. Of the measurements, 98.8% were in zones A and B in the CEG (as presented in Figure 3c and Table 1).

Postmarketing evaluation

Figure 4 depicts the graphs of two postmarketing users from Japan. The graphs are describing the correlation between the noninvasive CoG component and the references measurements over time. Three reference devices were used: the invasive CoG add-on meter, FreeStyle Lite (Abbott Laboratories, Alameda, CA), and Accu-Chek Aviva (Roche, Indianapolis, IN). As can be seen, there was good agreement between the noninvasive CoG device and the reference meters. Table 2 presents the MARD and the positive and negative MRD from this observation. The MARD between the CoG and the comparator devices: invasive CoG add-on meter, FreeStyle, and Accu-Chek was 11.2%, 12.7%, and 11.6%, correspondingly. Measured glucose levels were 117-238 mg/dL (157 ± 28), 112-264 mg/dL (162 ± 36), 106-290 mg/dL (161 ± 40), and 113-297 mg/dL (164 ± 40) for the noninvasive CoG, invasive CoG add-on meter, FreeStyle, and Accu-Chek, correspondingly. The positive and negative MRD and their diffusion (as presented in Table 2) showed a quite symmetrical diffusion around the regression line.

Discussion

This article is intended to present the novel noninvasive CoG device and its mathematical model for computing and

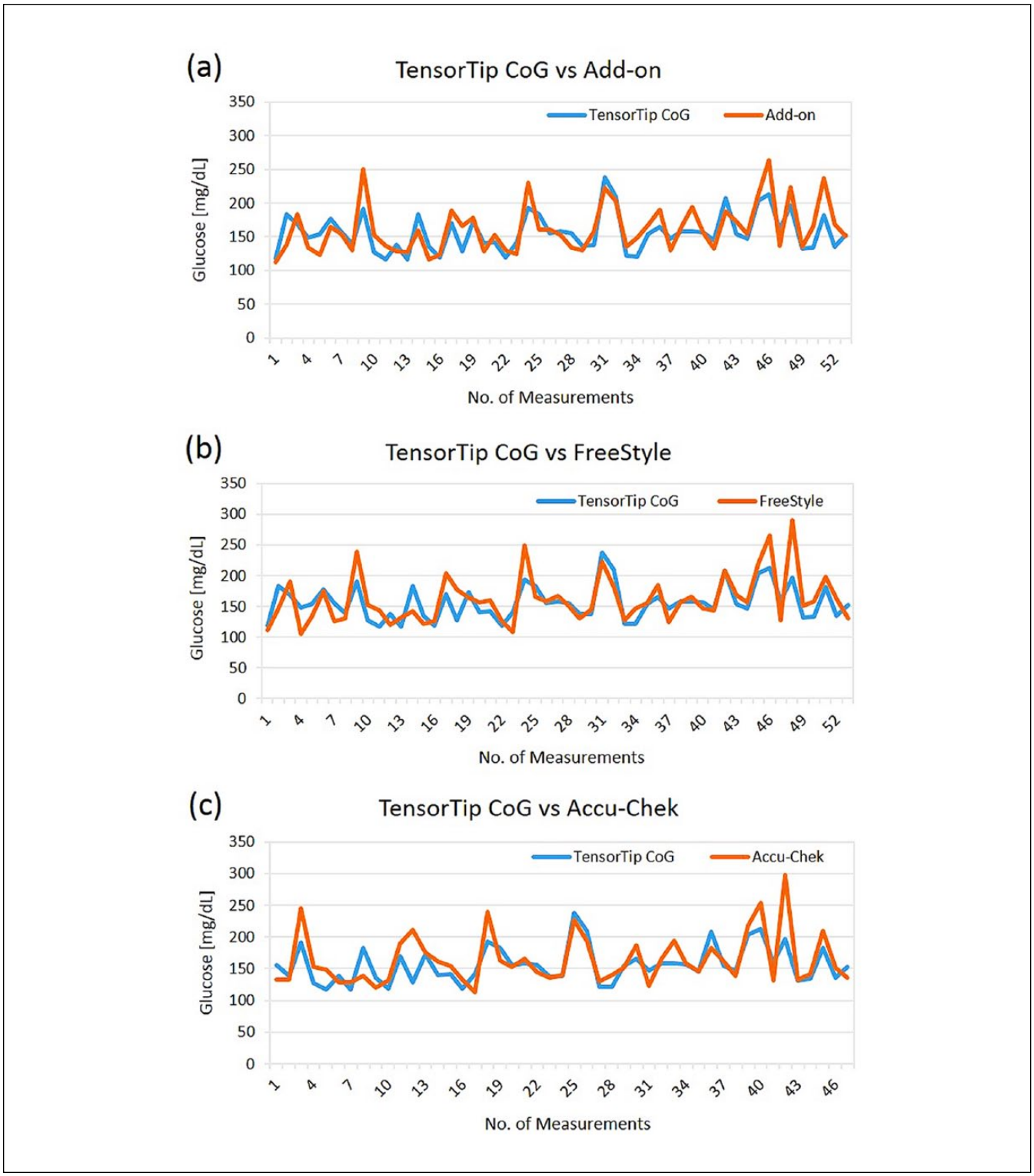

Figure 4. Individual patient readings in the postmarketing evaluation in comparison to the (a) invasive CoG add-on component, (b) FreeStyle, and (c) Accu-Chek.

predicting glucose capillary tissue levels. The noninvasive device technology provides a way to predict noninvasive capillary tissue glucose based on the change of the blood capillary momentary tint by employing a proprietary mathematical NBN machine to achieve *order* out of *disorder* by identifying groups of synchronized neurons in their

Table 2. Postmarketing Evaluation—Comparison of CoG Versus Several Comparator Devices.

CoG versus reference devices	MARD		Positive MRD			Negative MRD		
	Error (%)	Measurements (n)	Error (%)	Measurements (n)	Diffusion	Error (%)	Measurements (n)	Diffusion
Add-on	11.2	53	10.5	24	0.45	−11.9	29	0.55
FreeStyle	12.7	53	13.3	24	0.45	−12.2	29	0.55
Accu-Chek	11.6	47	11.2	19	0.40	−11.9	28	0.60

reactions. The combination of a multiple optical sensing technology with this novel and innovative mathematical algorithm has finally resulted in a medical device, which is capable to predict capillary tissue glucose concentrations with high quality. The underlying technology is also capable to collect and predict additional body signals such as hemodynamics, including blood pressure, pulse, stroke volume, cardiac output; blood gases, including pH, pCO_2, pO_2, HCO_3; hematology, including hemoglobin, RBC, HCT, and so on, which is currently subject to a second medical product (TensorTip MTX device)[30,34,35] independent from the CoG device presented in this article. The TensorTip family has similar hardware and mechanical design, however each bioparameter under consideration has a dedicated software procedure. This structure is similar to a PC where various software packages are executed on a similar platform.

During the development process, the noninvasive device was evaluated clinically in few medical centers and also by home users. Although the technology was compared to whole blood glucose results rather than capillary tissue glucose, the outcome from the initial studies presented in this article is sufficiently adequate to consider this new device for glucose prediction in daily routine with 98-100% of the paired data sets to be located in CEG zones A+B. The device is approved as a glucose monitoring tool in over 37 countries including the EU, China, Brazil, Israel, Philippines, Turkey, and others. In the meantime, additional studies have confirmed an even improved quality of the capillary tissue glucose prediction achieved by the CoG device. The results of a recent study in patients with type 1 diabetes, type 2 diabetes, and healthy subjects, where a standardized meal experiment was used to evaluate the noninvasive CoG performance in comparison to several comparators and a standard reference method, are reported by Pfützner et al in the same journal.[31]

Our goal was to develop a noninvasive device for an accurate prediction of capillary tissue glucose with a good and reliable performance as compared to common invasive methods. Initial clinical studies have already provided encouraging results, and more confirmatory studies are currently under way in different patient populations. This noninvasive technology is offering the opportunity for pain-free glucose monitoring in diabetes patient populations.

Appendix

A Brief Discussion of Photodetectors

In the appendix, we describe the distribution functions of light absorbed by the human retina photoreceptors called cones and probes. We focus on the cones.

Let $\mathbf{a_i(C)}$ represent the spectral color response absorbed by the retina. Three cones receptors have the spectra absorption distribution of $S_i(\lambda)$ i = 1,2,3 respectively with certain overlapping between the absorption distribution functions (particularly between S_1 and S_2, ie, Red and Green). The visible color sensation is defined in the range: $\lambda_{min} \le \lambda \le \lambda_{max}$ where $\lambda_{min} \cong 380\ nm$ and $\lambda_{max} \cong 780\ nm$, and described by the spectral responses:

$$\boldsymbol{a_i}(\boldsymbol{C}) = \int_0^\infty \boldsymbol{S_i}(\lambda)\boldsymbol{C}(\lambda)\boldsymbol{d}\lambda \tag{A1}$$

The retina cones visual spectra distributions of S_1,S_2 and S_3 decays outside the spectral bandwidth $[\lambda_{min}, \lambda_{max}]$. From eq. (A1) we can learn that two spectral distribution $C(\lambda_1)$ and $C(\lambda_2)$ may produce identical spectral response $a_i(C_1) = a_i(C_2)$ for i = 1,2,3. This means that two colors that look identical could have different spectral distribution.

In using primary colors, we observe from (A1) that the color matching coefficients h_{ij} are computed as follows:

$$\boldsymbol{h_{ij}} = \boldsymbol{a_i}(\boldsymbol{P_k}) = \int_0^\infty \boldsymbol{S_i}(\lambda)\boldsymbol{P_k}(\lambda)\boldsymbol{d}\lambda \ \text{k} = 1, 2, 3 \tag{A2}$$

Where each primary color distribution (k = 1,2,3) represents one of the basic colors (R, G or B) or any other suitable set of basic colors. In addition, we assume that each of the basic colors has a uniform energy distribution, that is, the integral over the domain λ_{min} to λ_{max} is unity. Hence, a color matching procedure involves solving the following equations:

$$\sum_{k=1}^{3} \varepsilon_k h_{ik} = \boldsymbol{a_i}(\boldsymbol{C}) = \int_0^\infty \boldsymbol{S_i}(\lambda)\boldsymbol{C}(\lambda)\boldsymbol{d}\lambda \tag{A3}$$

This means, for three primary colors P_1,P_2 and P_3 and three types of the retina (cones) distribution functions $S_i(\lambda)$ the coefficient matrix is computed from the cross correlation distribution response given in (A1) and (A2). Given three numbers ε_k the linear combination set in (A3) describes the color perceived as $C(\lambda)$.

The idea of color matching in the biophotodetector array (retina cones) is somehow adopted to the physical photodetector array in the sense of the sensitivity to wavelength (ie, colors—red, green, and blue) and not to the array distribution, while in the retina it distributes nonequispaced, in the CCD or CMOS photodetector array it distributes equispaced. Without loss of generality we assume that a photodetector array has a $D_i(x,y,\lambda)$ color distribution function (i = 1,2,3) for the three photodetector array marked as R,G,B (could be any other finite set of colors or equivalent distribution functions). Let $I(\lambda,x,y)$ be the color intensity distribution object. The coordinate system (x,y) represents the photodetector coordinate system or the film coordinate system where every space point (X,Y,Z) represents the 3D real-time manifold or real-time scenario or environment is projected onto the film coordinate system having the following projection coordinate connections

$$x = \xi \frac{X}{Z}, y = \xi \frac{Y}{Z}, \tag{A4}$$

where ξ represents the focal length of the film plane.

The photodetector array distribution response function is given mutatis mutandis to (A1) as follows:

$$\sum_{k=1}^{3} v_k(x,y)\, q_{ik}(x,y) = \boldsymbol{g_i}(\boldsymbol{x},\boldsymbol{y},\boldsymbol{I}) = \int_0^{\infty} \boldsymbol{D_i}(\boldsymbol{x},\boldsymbol{y},\lambda)\, \boldsymbol{I}(\boldsymbol{x},\boldsymbol{y},\lambda) d\lambda \tag{A5}$$

Where $g_i(x,y,I)$ represent the (x,y) photodetector cell response to the object I. Marking by R = $g_1(x,y,I)$, G = $g_2(x,y,I)$ and B = $g_3(x,y,I)$ the cell response to the object I respectively is D_1 for R, D_2 for G and D_3 for B of the photodectector array. The distribution functions decay outside a finite range, usually about 300 nm to 800 nm, for IR it is over 1200 nm and in case of thermo it is around 4000 nm.

Abbreviations

CEG, consensus error grid; CoG, Combo Glucometer; DSP, digital signal processor; MARD, mean absolute relative difference; MMMC, Memorial Morristown Medical Center; MRD, mean relative difference; NBN, neural brain network; PPG, photoplethysmogram.

Acknowledgments

The author would like to thank Prof Eli Zuckerman, head of the liver department in the Carmel & Lin Medical Centers, Dr Frank Smart from MMMC of the Atlantic Health System, and both their institutes for their help and support during the clinical studies. BIRD Foundation (Israel-U.S. Binational Industrial Research and Development Foundation) and Texas Instruments are highly appreciated for their valuable support in the development of the TensorTip CoG device. In addition, the author greatly acknowledges Alex Ternerider, Hisham Bishara, Dani Vainshenker, and Dana Segev for their significant role in the development of the device. Special thanks to Dr Ella Sheiman and Angel Mao for their contribution in certifying the device in China and Michal Shasha and Tova Hallas for their valuable contribution to this article.

Declaration of Conflicting Interests

The author(s) declared the following potential conflicts of interest with respect to the research, authorship, and/or publication of this article: YS is the inventor of the presented TensorTip CoG technology and founder of Cnoga Medical Ltd, the company commercializing the related products.

Funding

The author(s) received no financial support for the research, authorship, and/or publication of this article.

References

1. Ogurtsova K, da Rocha Fernandes JD, Huang Y, et al. IDF diabetes atlas: global estimates for the prevalence of diabetes for 2015 and 2040. *Diabetes Res Clin Pract*. 2017;128:40-50.
2. Valencia WM, Florez H. How to prevent the microvascular complications of type 2 diabetes beyond glucose control. *BMJ*. 2017;356:i6505. doi:10.1136/BMJ.I6505
3. Diabetes Control and Complications Trial Research Group, Nathan DM, Genuth S, et al. The effect of intensive treatment of diabetes on the development and progression of long-term complications in insulin-dependent diabetes mellitus. *N Engl J Med*. 1993;329(14):977-986.
4. Holman R, Paul S, Bethel M, Matthews DR, Neil HA. 10-year follow-up of intensive glucose control in type 2 diabetes. *N Engl J Med*. 2008;359(15):1577-1589.
5. Montagnana M, Caputo M, Giavarina D, Lippi G. Overview on self-monitoring of blood glucose. *Clin Chim Acta*. 2009;402(1-2):7-13.
6. Vaddiraju S, Burgess DJ, Tomazos I, Jain FC, Papadimitrakopoulos F. Technologies for continuous glucose monitoring: current problems and future promises. *J Diabetes Sci Technol*. 2010;4(6):1540-1562.
7. Girardin C, Huot C, Gonthier M, Delvin E. Continuous glucose monitoring: a review of biochemical perspectives and clinical use in type 1 diabetes. *Clin Biochem*. 2009;42(3):136-142.
8. Keenan DB, Mastrototaro JJ, Voskanyan G, Steil GM. Delays in minimally invasive continuous glucose monitoring devices: a review of current technology. *J Diabetes Sci Technol*. 2009;3(5):1207-1214.
9. Rodbard D. Continuous glucose monitoring: a review of successes, challenges, and opportunities. *Diabetes Technol Ther*. 2016;18(suppl 2):S3-S13.
10. Klonoff DC, Ahn D, Drincic A. Continuous glucose monitoring: a review of the technology and clinical use. *Diabetes Res Clin Pract*. 2017;133:178-192.
11. Vashist SK. Non-invasive glucose monitoring technology in diabetes management: a review. *Anal Chim Acta*. 2012;750:16-27.
12. Qu JY, Wilson BC. Monte Carlo modeling studies of the effect of physiological factors andother analytes on the determination of glucose concentration in vivoby near infrared optical absorption and scattering measurements. *J Biomed Opt*. 1997;2(3):319-325.
13. Shao J, Lin M, Li Y, et al. In vivo blood glucose quantification using Raman spectroscopy. *PLOS ONE*. 2012;7(10):e48127.

14. So C-F, Choi K-S, Wong TK, Chung JW. Recent advances in noninvasive glucose monitoring. *Med Devices (Auckl)*. 2012; 5:45-52.
15. Lipson J, Bernhardt J, Block U, et al. Requirements for calibration in noninvasive glucose monitoring by Raman spectroscopy. *J Diabetes Sci Technol*. 2009;3(2):233-241.
16. Sodickson LA, Block MJ. Kromoscopic analysis: a possible alternative to spectroscopic analysis for noninvasive measurement of analytes in vivo. *Clin Chem*. 1994;40(9):1838-1844.
17. Amerov AK, Arnold MA. In vitro kromoscopic analysis of glucose in blood. In: Priezzhev AV, Cote GL, eds. *Proceedings of the SPIE*. Vol. 4965. International Society for Optics and Photonics; 2003:7-16. doi:10.1117/12.479255
18. Yamakoshi Y, Matsumura K, Yamakoshi T, et al. Side-scattered finger-photoplethysmography: experimental investigations toward practical noninvasive measurement of blood glucose. *J Biomed Opt*. 2017;22(6):67001.
19. Yamakoshi T, Lee J, Matsumura K, et al. Integrating sphere finger-photoplethysmography: preliminary investigation towards practical non-invasive measurement of blood constituents. *PLOS ONE*. 2015;10(12):e0143506.
20. Haxha S, Jhoja J. Optical based noninvasive glucose monitoring sensor prototype. *IEEE Photonics J*. 2016;8(6):1-11.
21. Segman Y. Apparatus for obtaining and electronically interpreting digital images of liquids, solids and combinations on liquids and solids. United States patent US7728873B2. 2010.
22. Segman Y. Combination non-invasive and invasive bioparameter measuring device. United States patent US8948833B2. 2015.
23. Segman Y. Optical sensor device and image processing unit for measuring chemical concentrations, chemical saturations and biophysical parameters. United States patent US8335550B2. 2012.
24. Segman Y. Finger deployed device for measuring blood and physiological characteristics. United States patent US8489165B2. 2013.
25. Segman Y. Optical sensor device and image processing unit for measuring chemical concentrations, chemical saturations and biophysical parameters. United States patent US8792948B2. 2014.
26. Segman Y. Optical sensor device and image processing unit for measuring chemical concentrations, chemical saturations and biophysical parameters. United States patent US9402546B2. 2016.
27. Sinex JE. Pulse oximetry: principles and limitations. *Am J Emerg Med*. 1999;17(1):59-66.
28. Mendelson Y. Pulse oximetry: theory and applications for noninvasive monitoring. *Clin Chem*. 1992;38(9):1601-1607.
29. Kelleher JF. Pulse oximetry. *J Clin Monit*. 1989;5(1):37-62.
30. Segman Y. New method for computing optical hemodynamic blood pressure. *J Clin Exp Cardiol*. 2016;7(12):1-7.
31. Pfützner A, Strobl S, Demircik F, et al. Evaluation of a new noninvasive glucose monitoring device by means of standardized meal experiments [published online ahead of print February 1, 2018]. *J Diabetes Sci Technol*. doi:10.1177/1932296818758769
32. Parkes J, Slatin S, Pardo S, Ginsberg B. A new consensus error grid to evaluate the clinical significance of inaccuracies in the measurement of blood glucose. *Diabetes Care*. 2000; 23(8):1143-1148.
33. Pfützner A, Klonoff DC, Pardo S, Parkes JL. Technical aspects of the Parkes error grid. *J Diabetes Sci Technol*. 2013;7(5):1275-1281.
34. Segman YJ, Trahtemberg U. Oximeter behavior while using a tourniquet. *J Clin Exp Cardiolog*. 2016;7(11):1-2.
35. Yannan F, Deqing W, Yang Y. Case study for two noninvasive devices measuring hemoglobin. *J Clin Med Case Stud*. 2017;2(4):1-4.